The EMBO Journal (2004) 23, 2468–2477 | © 2004 European Molecular Biology Organization | All Rights Reserved 0261-4189/04
www.embojournal.org

THE EMBO JOURNAL

A new α-helical extension promotes RNA binding by the dsRBD of Rnt1p RNAse III

Nicolas Leulliot[1], Sophie Quevillon-Cheruel[1], Marc Graille[1], Herman van Tilbeurgh[1], Thomas C Leeper[2], Katherine S Godin[2], Thomas E Edwards[2], Snorri TL Sigurdsson[2], Natasha Rozenkrants[3], Roland J Nagel[3], Manuel Ares Jr[3] and Gabriele Varani[2,4,*]

[1]Institut de Biochimie et de Biophysique Moléculaire et Cellulaire (CNRS-UMR 8619), Université Paris-Sud, Orsay, France, [2]Department of Chemistry, University of Washington, Seattle, WA, USA, [3]RNA Center, Department of Molecular, Cell and Developmental Biology, Sinsheimer Laboratories, University of California, Santa Cruz, CA, USA and [4]Department of Biochemistry, University of Washington, Seattle, WA, USA

Rnt1 endoribonuclease, the yeast homolog of RNAse III, plays an important role in the maturation of a diverse set of RNAs. The enzymatic activity requires a conserved catalytic domain, while RNA binding requires the double-stranded RNA-binding domain (dsRBD) at the C-terminus of the protein. While bacterial RNAse III enzymes cleave double-stranded RNA, Rnt1p specifically cleaves RNAs that possess short irregular stem-loops containing 12–14 base pairs interrupted by internal loops and bulges and capped by conserved AGNN tetraloops. Consistent with this substrate specificity, the isolated Rnt1p dsRBD and the 30–40 amino acids that follow bind to AGNN-containing stem-loops preferentially *in vitro*. In order to understand how Rnt1p recognizes its cognate processing sites, we have defined its minimal RNA-binding domain and determined its structure by solution NMR spectroscopy and X-ray crystallography. We observe a new carboxy-terminal helix following a canonical dsRBD structure. Removal of this helix reduces binding to Rnt1p substrates. The results suggest that this helix allows the Rnt1p dsRBD to bind to short RNA stem-loops by modulating the conformation of helix α1, a key RNA-recognition element of the dsRBD.

The EMBO Journal (2004) **23,** 2468–2477. doi:10.1038/sj.emboj.7600260; Published online 10 June 2004
Subject Categories: structural biology; RNA
Keywords: dsRBD; RNA maturation; RNA–protein interaction; RNAse III; structure

Introduction

Eukaryotic orthologs of the prokaryotic ribonuclease RNAse III are endoribonucleases involved in the maturation of several classes of RNAs, including small nuclear (snRNAs) and small nucleolar RNAs (snoRNAs), as well as ribosomal RNA precursors (Elela *et al*, 1996; Chanfreau *et al*, 1998; Filipowicz and Pogacic, 2002). The yeast RNAse III (Rnt1p) has been proposed to participate in pre-mRNA turnover (Danin-Kreiselman *et al*, 2003), while *Dicer* and *Drosha* participate in higher eukaryotes in the processing of microRNAs and RNAi precursors (Knight, 2001; Lee *et al*, 2003). While most cellular nucleases cut single-stranded RNAs, RNAse III enzymes cleave double-stranded RNA (dsRNA) (Zamore, 2001; Conrad and Rauhut, 2002) using a conserved catalytic domain (Blaszczyk *et al*, 2001; Zamore, 2001). The specificity for dsRNA structures is provided by C-terminal dsRNA-binding domains (dsRBD), a class of universal dsRNA-binding motifs (Green and Matthews, 1992; St Johnston *et al*, 1992; Fierro-Monti and Mathwes, 2000).

Prokaryotic RNAse III enzymes cleave RNA duplexes regardless of sequence provided they are longer than 12–15 base pairs (bp). In contrast, the substrates of eukaryotic RNAse III (e.g. Rnt1p, *Drosha* and *Dicers*) are not generic dsRNAs: different classes of RNAse III orthologs have distinct substrate specificities (Lee *et al*, 2003). Rnt1p substrates are best characterized: the protein recognizes and processes imperfect stem-loops of 12–15 bp containing bulges and internal loops capped by AGNN tetraloops (Elela *et al*, 1996; Chanfreau *et al*, 1998, 2000; Nagel and Ares, 2000; Lebars *et al*, 2001; Wu *et al*, 2001; Lamontagne *et al*, 2003). The processing site appears to be determined in a ruler-like fashion: the RNAs are precisely cleaved 12–14 bp from the tetraloop-capping base pair (Chanfreau *et al*, 2000). Thus, eukaryotic RNAse III enzymes have evolved the ability to recognize RNAs with specific structural features and bypass the requirement for long RNA duplexes. Structures of AGNN tetraloops have been reported and have revealed a conserved structure (Lebars *et al*, 2001; Wu *et al*, 2001), but it is still unclear how Rnt1p recognizes this particular loop. It has been shown, however, that the Rnt1p dsRBD and the region of the protein C-terminal to it recapitulate the protein specificity in the absence of the catalytic domain (Nagel and Ares, 2000). The same domain of Rnt1p has also been proposed to mediate protein–protein interactions with Gar1p (Tremblay *et al*, 2002), a small nucleolar RNA component involved in other aspects of ribosomal RNA maturation (Dragon *et al*, 2000; Filipowicz and Pogacic, 2002).

Isolated dsRBDs recognize the length and structure of dsRNA tracts and discriminate effectively against DNA or DNA–RNA hybrids (Bevilacqua and Cech, 1996), but do not distinguish RNAs based on their sequence. However, dsRBD-containing proteins, especially the eukaryotic RNAse III enzymes, generally act on specific mRNAs in the cell (St Johnston *et al*, 1992; Polson and Bass, 1994; Proud, 1995; Lehmann and Bass, 2000; Nanduri *et al*, 2000): this is somewhat paradoxical. The structures of several dsRBDs (Bycroft *et al*, 1995; Kharrat *et al*, 1995; Nanduri *et al*, 1998) and of three protein–RNA complexes (Ryter and Schultz, 1998; Ramos *et al*, 2000b; Blaszczyk *et al*, 2004) have revealed

*Corresponding author. Departments of Chemistry & Biochemistry, University of Washington, Seattle, WA 98185-1700, USA.
Tel.: +1 206 543 7113; Fax: +1 206 685 8665;
E-mail: varani@chem.washington.edu

Received: 14 January 2004; accepted: 10 May 2004; published online: 10 June 2004

how the domain recognizes dsRNA. The motif has αββββα fold and two regions make structure-specific interactions with RNA double helices. Loop 2 (between β1 and β2) interacts with the RNA minor groove, while the C-terminal helix α2 and the Lys-rich preceding loop interact with phosphates across the major groove from the site of loop 2 interactions. The role of the third site of contact, helix α1, is less clear. In the two crystal structures (where different proteins were bound to the same RNAs), the helix interacts with the minor groove of a second RNA double helix presented to the protein by crystallographic packing interactions (Ryter and Schultz, 1998; Blaszczyk *et al*, 2004). In the NMR structure, helix α1 interacts instead with a tetraloop capping the dsRNA helix (Ramos *et al*, 2000b). It was suggested that interactions mediated by helix α1 (which is probably an evolutionary addendum to the dsRBD fold as it evolved from ribosomal protein S5; Bycroft *et al*, 1995) allow for specific interactions between at least some dsRBDs and RNA (Ramos *et al*, 2000b). If this mode of interaction was shown to be more general, it would provide an attractive explanation for the ability of some dsRBDs to bind RNA selectively.

Here we report NMR and crystallographic structures of the Rnt1p RNA-binding domain. We identify a new structural element, a C-terminal helix α3, abutting the N-terminal helix α1. We provide structural and biochemical evidence that this new helix is involved in the recognition of Rnt1p substrates by this enzyme by defining the conformation of helix α1.

Results

RNA-binding activity of Rnt1p requires the C-terminal region following the dsRBD

In order to probe the RNA-binding requirements of Rnt1p, we prepared several protein constructs (hereafter referred to as dsRBD (residues 364–435), medium-dsRBD (residues 364–447) and long-dsRBD (residues 364–471)) (Figure 1A). We also prepared oligonucleotide models of natural Rnt1 substrates consisting of perfect duplex of 14 bp capped by either AGGA or GUGA loops (as specificity control) and containing a single-stranded U overhang that mimics the natural Rnt1 cleavage products (Figure 1B).

As previously reported, the Rnt1p long-dsRBD constructs retain the RNA-binding specificity of the full-length protein (Nagel and Ares, 2000). The apparent K_d for the native stem-loop capped by an AGGA loop was 600 nM (Figure 2 and Table I); the K_d for the same duplex capped by a GUGA tetraloop was 2.25 μM, an approximately four-fold increase. Truncation of the C-terminus to within 17 amino acids of the canonical dsRBD (medium-dsRBD, amino acids 364–447) did not affect binding. NMR spectra of the constructs lacking the C-terminal tail were also identical, in the presence of RNA, to the spectra of the 364–447 construct. A further truncation to amino acid 433 to produce the short-dsRBD construct (corresponding to the deletion of helix α3, see below) reduced binding to both AGGA and GUGA constructs very significantly (Figure 2 and Table I). We conclude that amino acids 364–447 are both necessary and sufficient for recognition of short stem-loops capped by an AGGA tetraloop that

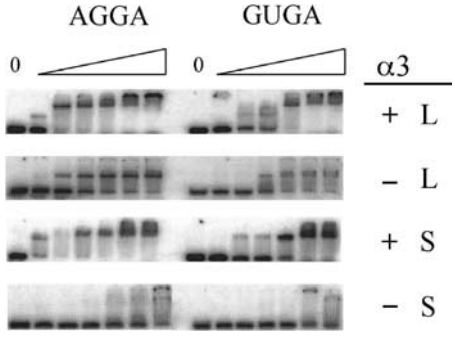

Figure 2 Band-shift analysis of the interaction between Rnt1p dsRBD protein constructs and RNA. The left panel reports the analysis of the interaction with AGGA containing either long (panels labeled L, 27 bp) or short (panels labeled S, 14 bp) RNA stem-loops, while the right panel reports the same analysis with GUGA mutants. Protein concentrations range from 0.5 to 10 μM (left to right). Two different protein constructs retain (+α3; residues 364–447) or lack (−α3; residues 364–433) helix α3.

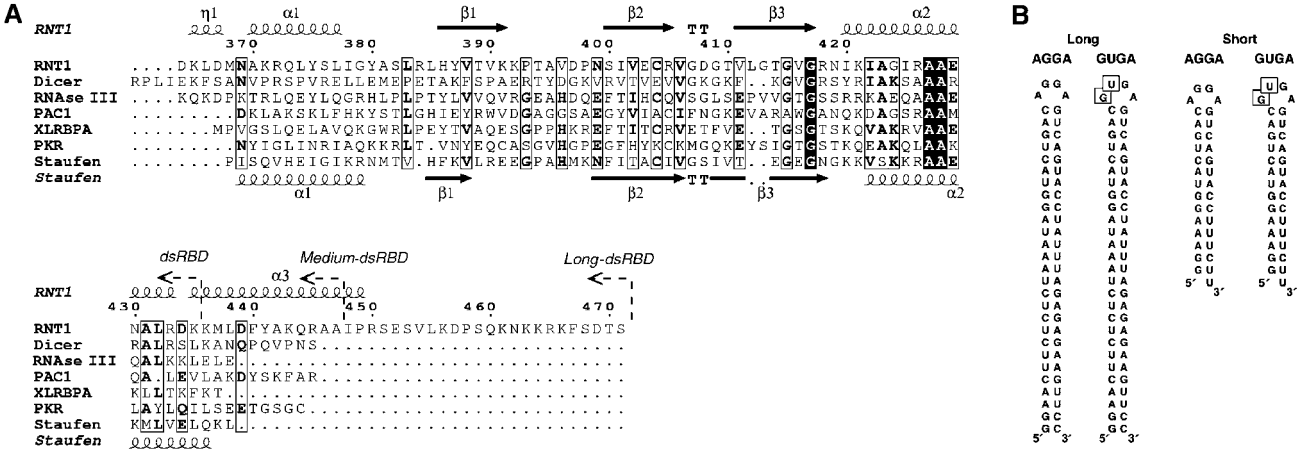

Figure 1 (**A**) Sequence alignment of Rnt1p dsRBD with dsRBD domains of RNAse III homologs Dicer (*Homo sapiens*), RNAse III (*E. coli*) and PAC1 (*Schizosaccharomyces pombe*) and with dsRBDs with available structural information, Xlrbpa (*Xenopus laevis*), PKR (*H. sapiens*), Staufen (*Drosophila melanogaster*); Rnt1p constructs studied in the present work are shown above the alignment. Secondary structures of Rnt1p (top) and Staufen (bottom) are indicated. Figure generated by ESPript (Gouet *et al*, 1999). (**B**) Secondary structure of the RNAs used in the present investigation.

Table I Apparent binding constants (μM) for Rnt1p–RNA interaction measured by gel shift assays as shown in Figure 2; long and short RNA constructs refer to stem-loops of 27 and 14 bp, respectively (Figure 1)

RNA protein	Long AGGA	Long GUGA	Short AGGA	Short GUGA
Long Rnt1p (364–471)	0.8	3.25	0.6	2.25
Short Rnt1p Δhelix 3	1.25	4.25	>10	>10
Stau dsRBD3	2.6	2.2	>10	>10

Protein constructs are defined in Figure 1 and in the text.

mimic physiological substrates of Rnt1p. Therefore, this region constitutes the minimal RNA-binding domain of Rnt1p.

In order to investigate more thoroughly the requirements for Rnt1p binding to RNA, we prepared two additional RNA constructs containing longer double helical stems of 27 bp. When probing the long-dsRBD construct with these long RNAs, K_d values of 0.8 and 3.25 μM were observed for AGGA and GUGA loops, respectively, comparable to those observed with the shorter substrate-like RNAs. However, the protein construct lacking helix α3 (see below) binds to these longer RNAs regardless of the presence or absence of the AGGA loop (Figure 2 and Table I). We attribute this result to the general dsRNA-binding ability of the dsRBD present in Rnt1p. This hypothesis is supported by the observation that Staufen dsRBD3, a well-known model for dsRBD–dsRNA interaction (Bycroft *et al*, 1995; Ramos *et al*, 2000b), is unable to bind to short RNA stem-loops (Table I) but binds to both AGGA- and GUGA-containing long RNAs with $K_d = 2.2$–2.6 μM (Table I). Furthermore, Rnt1p was recently shown to bind to but not cleave long RNAs regardless of the identity of the tetraloop (Lamontagne and Abou Elela, 2004). Altogether, these results suggest that the generic dsRNA-binding activity of the dsRBD on long double helical RNAs cannot compensate for the absence of specific interactions with the tetraloop.

Full-length Rnt1p binds RNA as a dimer (Lamontagne *et al*, 2000; Nagel and Ares, 2000) and it is virtually certain that the complete protein performs catalysis in the dimeric form as bacterial RNAse III does (Blaszczyk *et al*, 2001). However, it is unknown whether fragments containing just the dsRBD dimerize under native conditions in the presence of RNA. Constructs including residues 330–364 behaved similarly to the 364–471 protein, indicating that a conserved region (330–364), proposed to be involved in dimerization, contributes little to the binding. Since the stoichiometry of binding cannot easily be determined by band-shift analysis, we recorded ^{15}N-HSQC spectra at different protein–RNA ratios. When a 1:1 complex of Rnt1p and the AGGA-stem loop RNA was prepared, we observed significant chemical shift changes for about half of all amide resonances; no additional changes were observed when the protein concentration was increased further until, at much higher protein–RNA ratios, aggregation was progressively observed. Thus, the dsRBD of Rnt1p binds to RNA as a monomer.

Protein structure determination

The data presented above indicate that the Rnt1p fragment encompassing amino acids 364–447 (medium-dsRBD) region constitutes the minimal RNA-binding domain. The medium-dsRBD construct was therefore used for NMR structure determination. Standard triple-resonance experiments (Supplementary Table S1) were used to assign the spectrum of the free protein as described in Materials and methods. NOE distance restraints were subsequently obtained through the analysis of ^{15}N- and ^{13}C-edited NOESY spectra recorded at mixing times of 100 ms. Homonuclear NOESY experiments were also collected in D_2O in order to obtain NOE constraints for the aromatic protons, which were assigned from TOCSY spectra recorded under the same conditions. Hydrogen-bonded amides were established by recording HSQC spectra of a protein sample after rapid lyophilization in D_2O and by using preliminary structures to identify the bonding partner. Structure calculation carried out using both X-PLOR (Howe *et al*, 1998; Ramos *et al*, 2000a) and CNS (Brunger *et al*, 1998) yielded the same results. Structural statistics are presented in Table II.

For the purpose of X-ray crystallography, diffracting crystals could be obtained for two protein constructs (medium- and long-dsRBD), but X-ray diffraction data were recorded to 2.5 Å resolution only on crystals of the longer protein construct. The crystals belong to C2 space group with a solvent content compatible with two molecules in the asymmetric unit. The structure was solved by molecular replacement (MR) using the NMR ensemble of structures as a search model as described in Materials and methods. The final model contains two molecules per asymmetric unit, including residues 362–443 and 361–448, respectively; the r.m.s.d. between the two monomers (for C_α atoms only) is 0.67 Å. Since intermolecular interactions only cover a small surface area, dimerization in the crystal is most likely to be an artifact of crystal packing. Data acquisition and refinement statistics are presented in Table III.

Protein structure

Rnt1p adopts the same fold as all other dsRBDs with the canonical αββββα topology and the α1 and α2 helices packed

Table II NMR experimental constraints and structure statistics

Distance constraints	
Total	1424
Intraresidue	390
Medium range (<4 residues)	669
Long range (>4 residues)	309
Hydrogen bonds	56
Structure statistics	
NOE violations	
Number >0.2 Å	0
Maximum violation	0.15 Å
R.m.s.d. from average structured (Å)	
Regular secondary structure elements (residues 7–29, 37–45, 48–86)	
Backbone	0.52
Heavy atoms	1.52
Mean deviation from ideal covalent geometry	
Bond lengths	0.0016 Å
Bond angles	0.3346°
Impropers	0.1736°
Ramachandran analysis	
Most favored region	75%
Allowed region	23.9%
Disallowed region	1.1%

Table III Crystallographic analysis and refinement statistics

Data collection statistics	
Space group	C2
Wavelength	0.933 Å
Unit-cell parameters	$a = 73.81$, $b = 68.31$, $c = 57.19$ (Å)
	$\alpha = 90°$, $\beta = 121.9°$, $\gamma = 90°$
Resolution	48.8–2.5 Å
Number of reflections	23 103
Number of unique reflections	7943
Multiplicity	2.9
R_{merge}	7.1%
$I/\sigma(I)$	6.3
Overall completeness	94.3%
Refinement statistics	
Reflections (working/test)	7162/779
R_{cryst}/R_{free}	18.9%/28.3%
Non-hydrogen atoms	2755
Water molecules	23
Bonds (Å)	0.005
Angles (deg)	0.71
Mean *B*-factor (Å^2)	48.1
Ramachandran analysis	
Most favored	81.4%
Allowed	18.6%

against the antiparallel β-sheet (Figure 3). Unlike other dsRBDs, however, residues following the end of helix α2 are well structured and form a stable α-helix (α3, residues 436–447); the short loop between helices α2 and α3 (residues 433–435) forms a structurally well-defined rigid hinge. The same helical structure is observed in both constructs (365–447 and 363–471) by both NMR and crystallography, although in the X-ray structure electron density can only be observed up to residues 443 (or 448) in the two independent proteins in the asymmetric unit. Superposition of the NMR structure with the two independent crystal structures reveals residual positional flexibility of helix α3 reflecting both intrinsic positional heterogeneity and intermolecular crystal packing interactions (Figure 3C). However, helix α3 is as well defined as the other secondary structure elements: *B*-factors and NMR line widths within helix α3 and the hinge with helix α2 are comparable to those observed in other parts of the protein. The new helix makes extensive packing contacts with the rest of the protein (notably with residues Ile377, Ile378, Tyr380 and Leu383) that effectively lock helix α3 at both its N-terminus (with helix α2) and its C-terminus (with loop 1).

The structural data demonstrate that the new helix is an integral part of the Rnt1p dsRBD structure, although it does not form part of the canonical dsRBD fold. When we expressed constructs lacking helix α3, the protein became partially insoluble and NMR spectra were of poor quality. Both results suggest aggregation and/or partial unfolding of the protein when the helix is removed. The data presented in Table I and Figure 2 indicate that it also plays an important role in RNA binding. Helical appendices have been observed in several RRM proteins and have been demonstrated to participate in RNA recognition (Avis *et al*, 1996; Allain *et al*, 2000; Varani *et al*, 2000; Wang and Tanaka-Hall, 2001; Perez-Canadillas and Varani, 2003). However, this is the first report, as far as we are aware, of any augmentation of the dsRBD fold and of the participation of secondary structural elements outside the canonical dsRBD fold in RNA recognition.

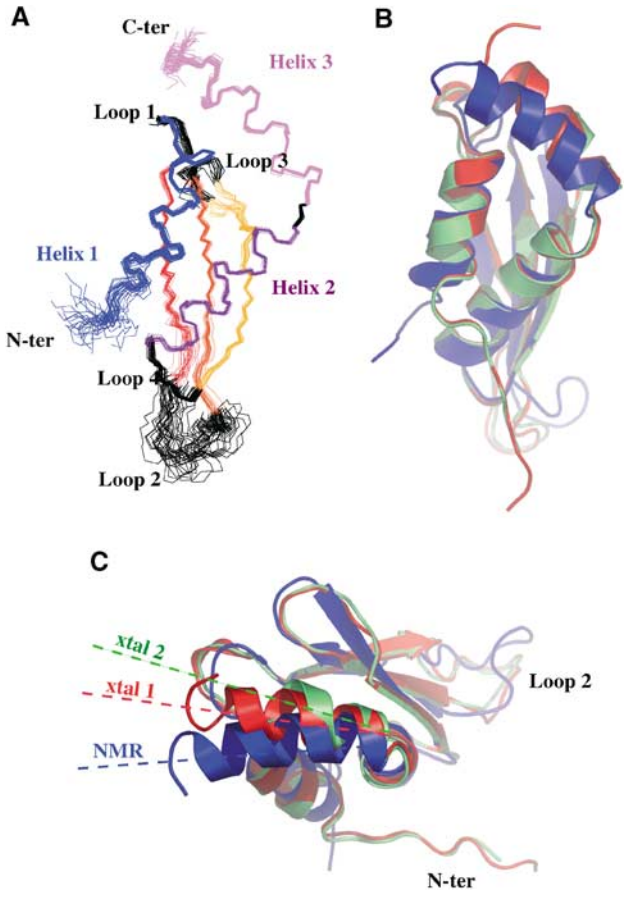

Figure 3 Rnt1p RNA-binding domain protein structure. (**A**) NMR ensemble; superposition of converged structures of RNA-free dsRBD with color-coded secondary structure elements: α1 blue, α2–α3 purple, β-sheet 1–3 red–orange–yellow, respectively. (**B, C**) Superpositions of NMR (blue) and two independent crystal structures (red and green, respectively). Helix α3 has slightly different orientation in each of the three structures (dashed line, C). Loop 2 and the N-terminal residues preceding helix α1 have a similar and well-defined conformation in both crystal structures but are flexible in solution.

Conformational flexibility of Rnt1p dsRBD

While the core of the dsRBD is rigidly defined, several regions of the Rnt1p RNA-binding domain are conformationally heterogeneous (Figures 3A and B). Loops 1–3 are flexible and several amide resonances from these loops could not be assigned: they are missing in the ^{15}N-HSQC or do not show any cross-peaks to other side-chain resonances. The corresponding residues show considerable conformational flexibility in the final ensemble of structures (Figure 3A). Although lack of NOE constraints is not proof of flexibility, the position of these residues and their behavior upon RNA binding (see below) lead us to believe that these residues are truly disordered in the free protein, as they were in Staufen (Ramos *et al*, 2000b). In the X-ray structures, loop 2 is rigid in one monomer (clear electron density is observed for all residues; Figure 4), while loop 2 of the second monomer has higher *B*-factors and poorer electron density. The smaller loops 1 and 3 are also better defined in the electron density compared to the solution conditions due to intermolecular interactions; their overall conformations, however, are similar to the average of the NMR ensemble (Figures 3B and C).

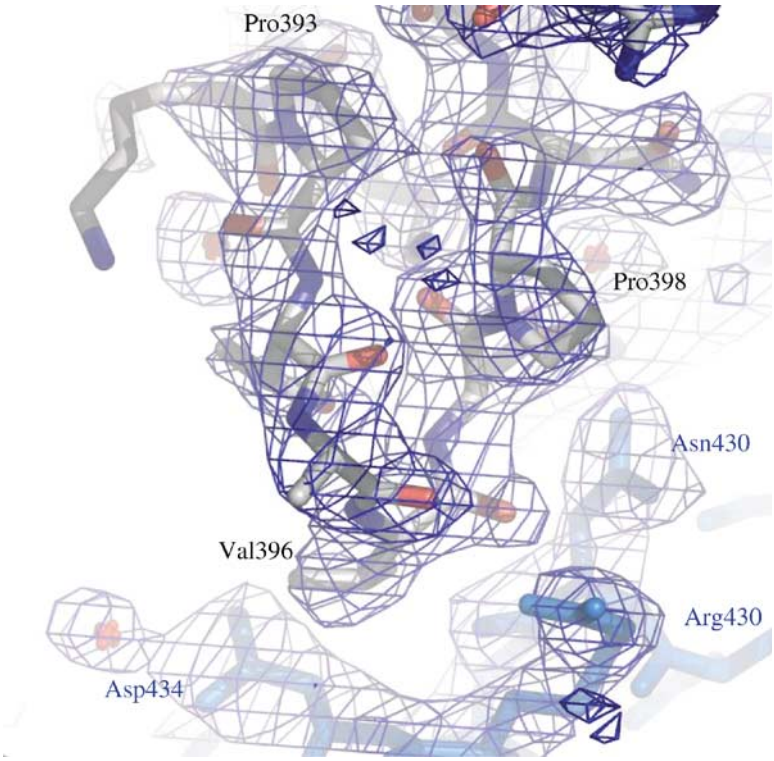

Figure 4 Structure of loop 2. The $2F_o$–F_c electron density map is contoured at 1σ. The flexible loop 2 in the NMR structure (Figure 3A) is stabilized in the X-ray structure by intermolecular interactions (indicated in blue sticks).

Loop 2 is a key RNA-binding element of the dsRBD (Ryter and Schultz, 1998; Ramos *et al*, 2000b). In free Rnt1p, it is oriented away from the RNA-binding surface (see below), as observed also in free Staufen dsRBD3 (Ramos *et al*, 2000b) and PKR (Nanduri *et al*, 1998). In the crystal, the loop 2 structures are stabilized by intermolecular crystal packing interactions with the middle of helix α3 and with the C-terminal part of helix α2 in each of the two copies of the structure, yet the two loops have very similar conformation and orientation. In solution, the loop retains flexibility about hinge residues at either end: two sets of NOESY cross-peaks are observed for Pro393 and another proline (Pro398) is present at the C-terminal end of the loop, suggesting that *cis-trans* isomerization may be responsible for the conformational flexibility of the loop. Only cross-peaks corresponding to the most populated conformer were used in the structure calculation and very little information could be gathered on the conformation of the second population. Upon RNA binding, however, only one set of resonances is observed for loop 2 and four amide resonances (from loops 1, 2 and 4) become clearly visible indicating a rigidification of the conformation of each of these loops. Loop 2 must rotate toward the RNA during binding. We suggest that the positively charged amino acids in loop 4 recruit the RNA first, then loop 2 clamps into the minor groove of the RNA to provide further affinity and lock the protein on the RNA. The flexibility of loop 2 may very well be a major determinant of the RNA-binding ability of this protein family. The RNA-binding activity of dsRBDs might have an important dynamic component: in the protein kinase PKR, dsRBD1 (which binds RNA with a greater affinity than dsRBD2) exhibits significant motional flexibility on the millisecond timescale, while dsRBD2 is more rigid (Nanduri *et al*, 1998, 2000).

RNA-binding interface of Rnt1p

Significant spectral changes are observed in the protein and RNA spectra upon complex formation (Figure 5). Observation of the same pattern of NOE interactions, however, demonstrates that the structural rearrangements upon RNA binding, if any indeed occur, are very small. The most remarkable spectral change upon RNA binding involves the Nε of the arginine side chains. In the free protein, only the Nε of Arg405 is visible; this residue is not located near the RNA-binding surface of the protein. In contrast, five additional Nε amide resonances corresponding to the missing arginine side chains become observable in the complex (Figure 5A). These five arginine residues either become ordered upon RNA binding and/or they become highly protected from solvent exchange through interactions with the RNA. While it has not been possible to assign these resonances to specific arginines (no NOEs could be observed between these Nε protons and other protons belonging to either protein or RNA residues), five arginines (Arg372, Arg384, Arg418, Arg426 and Arg445) are located on the binding interface determined by chemical shift mapping (see below), while Arg433 and Arg405 are not.

Because of increased protection from the solvent and rigidification of the loop structure, several resonances not observable in free Rnt1p could be unambiguously assigned in the RNA-bound protein and a more complete list of NOE constraints was collected. Structure calculations with this new list of constraints confirmed that the RNA-bound protein

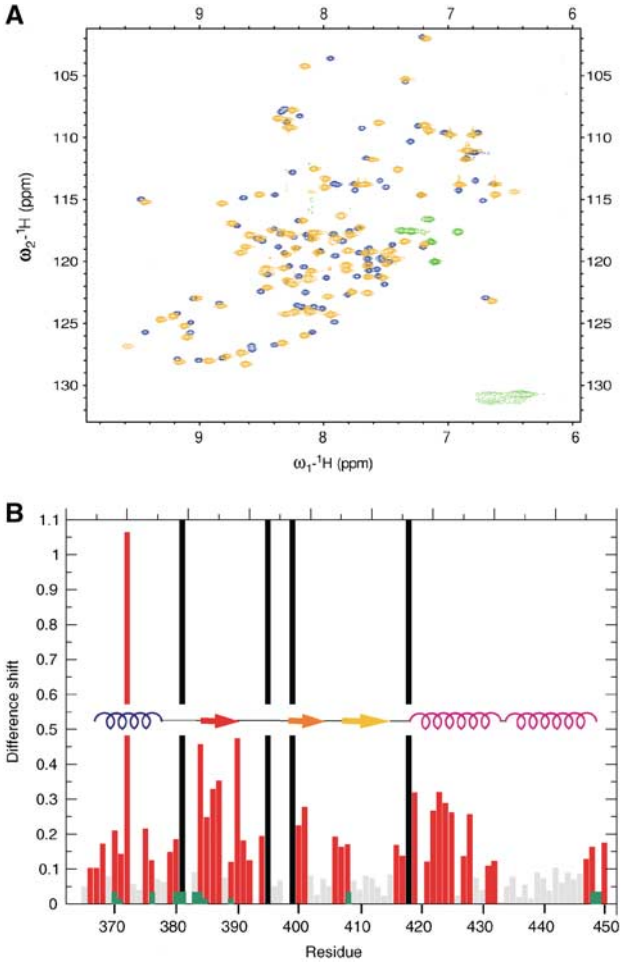

Figure 5 The interaction of Rnt1p medium-dsRBD with AGGA tetraloops. (**A**) ^{15}N-HSQC spectra of Rnt1 dsRBD free (blue) and bound to its cognate RNA (orange). Frequency folding of the spectrum makes arginine Nε resonances appear as negative peaks (green). Only Arg405 Nε is visible in the unbound state, but five Arg Nε resonances become clearly observable in the RNA-bound dsRBD. (**B**) Chemical shift differences between free and bound Rnt1p identifies the RNA-binding interface; the secondary structure is shown as well. The RNA-induced shift was calculated as the square root of the sum of the square of the ^{1}H and ^{15}N chemical shift difference; the ^{15}N chemical shift difference was downweighted by a factor of 10 to take into account the greater chemical shift range of protons. Resonances were considered shifted when the difference was greater than 0.1. Green bands correspond to resonances located in close proximity of the AGGA tetraloop by the spin-labeling experiment.

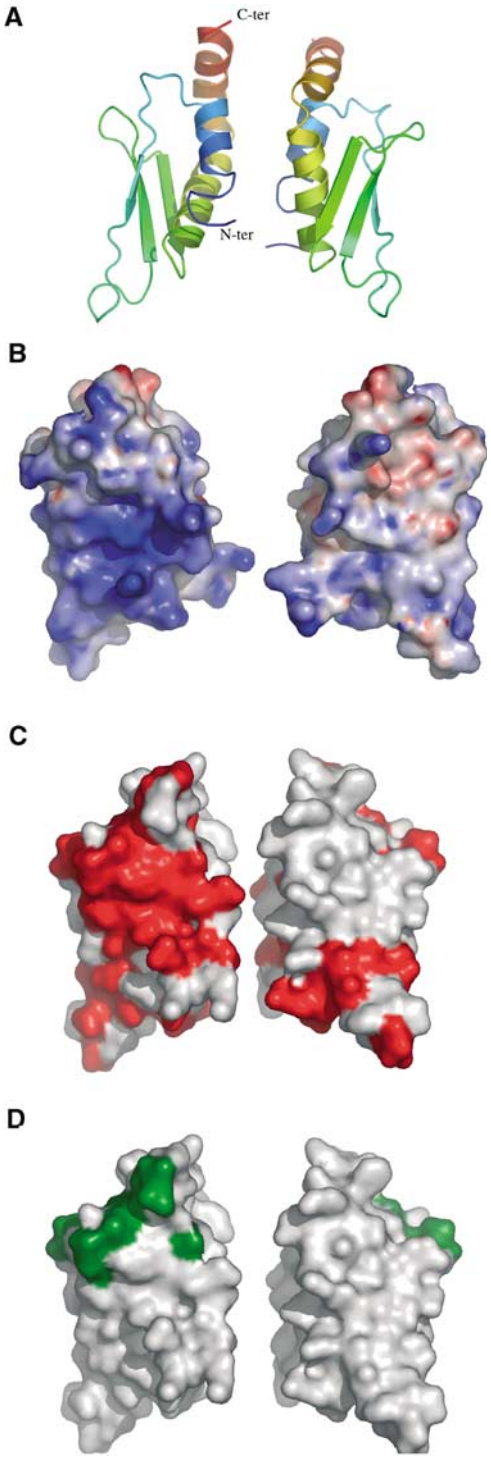

Figure 6 (**A**) RNA-free Rnt1p medium-dsRBD structure in the same orientations used in the surface representations. (**B**) A region of positive electrostatic potential on the surface of the Rnt1p dsRBD crystal structure (blue patches) coincides with the RNA-binding surface of the protein. (**C**) Residues that shift upon RNA binding identify the RNA-binding surface of Rnt1p (red-coded residues). (**D**) Residues located close to the AGGA tetraloop as identified in the spin-labeling experiments (green-coded residues). The tetraloop interaction site is precisely determined by the spin label experiment and coincides with helix α1, loop 1 and the C-terminus of helix α3.

adopts the same overall structure as free Rnt1p. Residues where large chemical shifts are observed upon RNA binding are mapped on the RNA-free Rnt1p structure in Figures 6A and C. Sites of interaction identified by this analysis include helix α1, loop 1, strand β1, loop 2 and the N-terminus of helix α2. The binding surface thus defined agrees very well with a ridge of positive electrostatic potential (Figure 6B) and with the binding interface determined for the two dsRBD/RNA complexes (Ryter and Schultz, 1998; Ramos *et al*, 2000b).

Helix α1 is proximal to the AGNN tetraloop

In order to establish the orientation of Rnt1p onto its RNA target, we attached a single paramagnetic label onto the RNA and observed close proximity of protein resonances to the site of attachment through electron–proton paramagnetic relaxation (Ramos and Varani, 1998; Ramos *et al*, 2000a, b). The nitroxide spin label was attached to the third nucleotide of an

AGUA tetraloop; this sequence is functionally equivalent to the AGAA loop used for most studies, but allows derivatization of the uracil base to be carried out using well-established chemistry. NMR spectra of the protein bound to both sequences were very similar, indicating that the protein binds both loops very similarly as well. HSQC spectra were recorded for the protein bound to derivitized RNA before and after reduction of the spin label. A few residue resonances that are broadened in the sample containing the unpaired electrons by electron–proton relaxation sharpen up significantly once the nitroxide label is reduced: Ala370, Lys371, Ser376, Tyr380, Ala381, Leu383, Arg384, Leu385, Thr389, Asp408, Ala448 and Leu449. This result unambiguously identifies protein resonances located within 12–15 Å of the site of labeling. Sites of the protein located in proximity of the tetraloop are identified on the RNA-free protein structure in Figure 6D. These data demonstrate that helix α1 is in close proximity to the tetraloop, a structural arrangement very similar to that observed in the Staufen complex (Ramos *et al*, 2000b).

Discussion

The yeast RNAse III, Rnt1p, processes short irregular stem-loops of 12–14 bp capped by conserved AGNN tetraloops, while prokaryotic RNAse III enzymes cleave long RNA duplexes regardless of their sequence. In an effort to understand the molecular determinants of the specificity of the yeast RNAse III, we have determined the structure of the Rnt1p RNA-binding domain using both NMR and X-ray crystallography. We have discovered that the dsRBD of Rnt1p is augmented by a new C-terminal α-helix. Helix α3 stabilizes the protein and is required to observe any significant binding to short stem-loops that mimic physiological Rnt1p substrates.

When the new helix was removed, partial insolubility and protein unfolding were observed. Furthermore, binding to short stem-loops that mimic Rnt1p substrates was no longer observed (Figure 2). The protein retains the ability to bind to long (27 bp) dsRNAs regardless of the new helix, probably because of the generic dsRNA-binding activity of the dsRBD. Staufen dsRBD3, a well-known model for the dsRBD, binds to long RNAs as well as Rnt1p dsRBD, but fails to bind to the shorter stem-loops (Table I). It has recently been shown as well that Rnt1p binds to but does not process long dsRNAs when the AGGA loop sequence is mutated (Lamontagne and Abou Elela, 2004). These studies indicate that the presence of helix α3 allows Rnt1p to bypass the requirement for long RNA duplexes and bind to short RNA stem-loops that mimic its physiological substrates.

Helix α3 is the most unusual feature of any dsRBD studied to date (Figure 7). The core structure of the dsRBD is remarkably well conserved, much more so than RRM structures (Varani and Nagai, 1998; Wang and Tanaka-Hall, 2001). While in RRMs the helices have variable length and orientations, the packing of helices α1 and α2 against the β-sheet is nearly identical in all dsRBD structures. The conformation of loop 4 and the N-terminus of helix α2 is also extremely well conserved. This loop and the two helices, together with loop 2, contain conserved positively charged residues involved in RNA binding (Ryter and Schultz, 1998; Ramos *et al*, 2000b). It was proposed that the distance between loops 4 and 2 is a critical determinant of the ability of the dsRBD to bind dsRNA selectively over dsDNA or DNA–RNA hybrids; the structural conservation shown in Figure 7 reinforces this suggestion.

What is the structural role of helix α3, and how does it affect RNA binding? There are only a few chemical shift changes in helix α3 upon RNA binding, suggesting that the helix does not interact extensively with the RNA, if at all. In fact, only the amino acids at the very C-terminus of helix α3

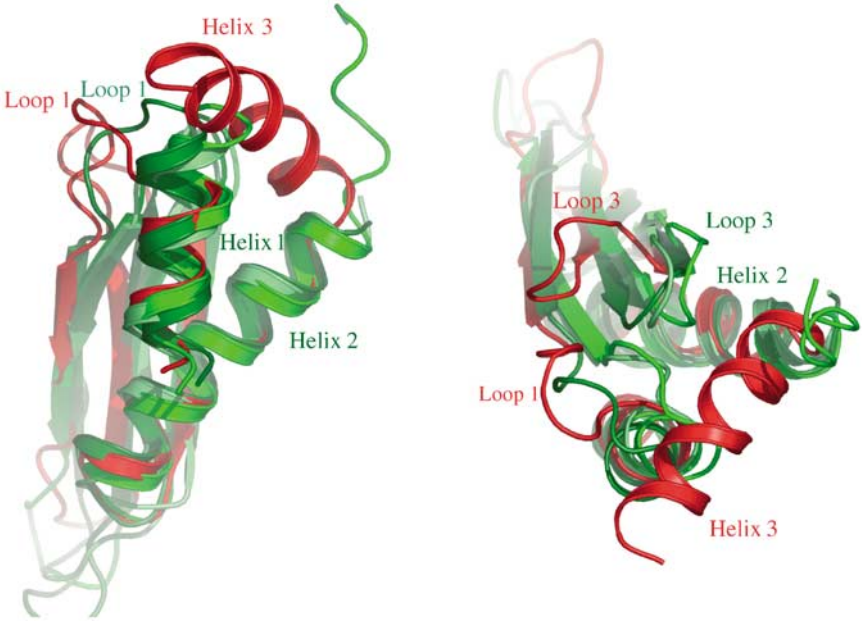

Figure 7 Superposition of the unbound Rnt1p medium-dsRBD NMR structure (red) with previously determined dsRBDs: Staufen (Ramos *et al*, 2000b), Xlrbpa dsRBD2 (Ryter and Schultz, 1998) and PKR dsRBD1 (Nanduri *et al*, 1998) (various shades of green). See Figure 1 for sequence alignment. The orientations of the α-helices as well as the β-sheet are very well conserved in all structures. However, the presence of the extra helix α3 in Rnt1p medium-dsRBD distorts helix α1, loop 1 and loop 3, thereby remodeling the structure of the RNA-binding interface.

point toward the RNA and are located close to the AGGA loop in the spin-labeling experiment (Figure 6D). If helix α3 does not contact RNA directly, how does it then contribute so significantly to RNA binding? Helix α3 packs against the region of the protein (helix α1/loop 1) that approaches the AGNN loop. We previously suggested that helix α1 could play a role in identifying specific substrates for at least some dsRBDs (Ramos *et al*, 2000b). The interaction of helix α3 with the C-terminal end of helix α1 and loop 1 would generate a sterical clash with the first helix if its length was the same as in the other dsRBDs. In order to accommodate the new helix, helix α1 is shortened and loop 1 protrudes more deeply toward the RNA-binding surface than observed in other dsRBDs. Thus, the presence of helix α3 induces a divergent structure for a key region of the interface by shortening helix α1 to a conformation that is unique among all dsRBDs studied so far (Figure 7). When we mutated Arg445–Ala, resonances within the extended hydrophobic patch packing helices α1 and α3 and within loop 1 were broadened or shifted, indicating a destabilization of this region of the protein. The Arg445–Ala mutant protein–RNA complex precipitated. These results suggest that the new helix contributes to RNA binding indirectly through its effect on the conformation of the helix α1–loop 1 region.

In summary, we have demonstrated that the ability of Rnt1p enzymes to bind to short stem-loops capped by AGGA loops that mimic its physiological substrates requires a new α-helical extension to the canonical dsRBD. Although the new helix does not participate directly in the recognition of the AGGA loop, the structural analysis strongly suggests that its interaction with helix α1/loop 1 is critical to position residues that are essential for RNA binding.

Materials and methods

RNA and protein expression and purification

RNAs used in the biochemical and structural investigations (Figure 1) were prepared by *in vitro* run-off transcription using T7 RNA polymerase and purified as described (Price *et al*, 1998). Several protein constructs were prepared as discussed in the text. DNAs corresponding to the various constructs were amplified using standard methods from yeast genomic DNA by standard PCR methods and inserted into pET21 or pET9 vectors. Cell cultures (BL21(DE3) *Escherichia coli*) were then grown in M9 minimal media supplemented with appropriately isotope-labeled NH_4Cl and ^{13}C-glucose, as required. Cultures were induced with IPTG during mid-logarithmic phase and harvested 4 h post-induction. Protein purification was conducted by metal chelate affinity chromatography. His tags (separated by two linker residues) were added to the C-or N-terminus to facilitate protein purification. The proteins were further purified by anion exchange followed by size exclusion chromatography. No impurities were detected either by SDS gel electrophoresis or by mass spectroscopy.

RNA-binding assays

End-labeled RNA was prepared and used for gel shift experiments as described (Nagel and Ares, 2000). Dried gels were exposed to a phosphorimaging plate and scanned with a phosphorimager; bands corresponding to free and bound RNA were quantified using *ImageQuant* software.

Optimization of experimental conditions

Experimental conditions for NMR were optimized in parallel for the free protein and for the protein–RNA complex to facilitate subsequent analysis. ^{1}H–^{15}N HSQC spectra were recorded under different conditions and the protein conformation was monitored by observing protein amide resonances. The pH had a notable effect; above 6.5, the number and spread of amide resonances were indicative of a well-structured protein, while below pH 6.5, an additional set of approximately eight peaks appeared in the HSQC spectra, indicating the presence of a second conformer. This behavior is probably due to local unfolding due to His protonation, but we made no attempt to characterize the secondary low pH conformer. Conditions used for recording NMR spectra were 10 mM phosphate buffer at pH 6.5, 1 mM DTT and 310 K.

NMR spectroscopy

NMR experiments were conducted on Bruker AV500, DMX600 and AV800 MHz spectrometers equipped with triple-resonance probes and gradient units. All experiments were performed under the same buffer conditions (10 mM phosphate (pH 6.5), 1 mM DDT) at a temperature of 310 K unless otherwise specified. The experiments used in the assignments of resonances of the free and bound protein are listed in Supplementary Table S1. Backbone Cα, Cβ, C′, N assignments were obtained using standard triple-resonance experiments (Sattler *et al*, 1999). 2D NOESY experiments (conducted in both H_2O and D_2O) at mixing times of 60, 120 and 300 ms recorded at 600 MHz and 3D ^{15}N-edited NOESY at a mixing time of 100 ms were used to obtain distance constraints. In order to determine which amide protons are involved in hydrogen bonds, the protein was lyophilized and rapidly re-suspended in D_2O. A ^{15}N-HSQC spectrum was collected immediately after re-suspension with the temperature lowered to 280 K to slow amide exchange with solvent (at the relatively high pH of our experiments, all amide resonances were fully exchanged at room temperature before spectra could be collected). Resonances that exchanged slowly enough to be protected from exchange were considered hydrogen-bonded. The hydrogen-bonded partners were determined using MOLMOL (Koradi *et al*, 1996) based on preliminary structures calculated using only NOE restraints. Slowly exchanging amides with ambiguous attribution of the bonded partner were not constrained. The assignment of the protein resonances of the RNA-bound protein was conducted in parallel with the protein structure calculation. Since about half of all amide resonances experience only small perturbations in their ^{15}N-HSQC and ^{13}C-HSQC spectra, it was possible to assign over half of the backbone and side chains of the RNA-bound protein by visual inspection based on the free protein assignments. In order to confirm these assignments and further assign all shifted resonances, we recorded three-dimensional ^{15}N-edited NOESY and TOCSY spectra of the complex. ^{13}C-edited NOESY as well as homonuclear NOESY and TOCSY spectra in D_2O were then used to complete the side-chain assignments.

NMR structure calculation

Structure calculations were performed starting from 50 randomly generated conformers that were then subjected to simulated annealing using an XPLOR protocol that has been successfully used for other protein/RNA complexes (Howe *et al*, 1998; Ramos *et al*, 2000a). Simulated annealing using torsional angle dynamics in CNS (3000 steps of TAD followed by cartesian dynamics during the slow cooling step) was also used due to the increased speed of these calculations (Brunger *et al*, 1998). The overall results were very similar using both protocols. Experimental data and structural statistics are summarized in Table II.

Identification of Rnt1p–AGNN contacts by paramagnetic relaxation

Well-established chemistry based on chemical synthesis of the RNA with 4-thio-uracil (Dharmacon) followed by reaction with 3-(2-iodoacetamido)-proxyl was used to attach a nitroxide spin label to the third base of the tetraloop (Ramos and Varani, 1998; Varani *et al*, 2000). Instead of AGAA, we used an AGUA loop that still conforms to the AGNN consensus; NMR spectra of the protein bound to the modified loop were very similar to those observed with the original AGAA loop. Progression of the labeling reaction was monitored by UV absorption at 320 nm; reacted RNA was separated from unreacted crude product by standard gel electrophoresis methods. Once a spin-labeled nitroxide is attached to the RNA, the unpaired electrons cause electron–proton paramagnetic relaxation by a dipolar mechanism; because the electron dipole is so large, relaxation effects extend to 15–20 Å (Gochin, 2000; Lugovskoy *et al*, 2002) and can be easily detected from the broadening or disappearance of protein resonances in the HSQC spectra (Ramos and Varani, 1998). Upon addition of a reducing agent such as sodium hydrosulfite, the normal spectrum was recovered thereby

allowing the unambiguous identification of protein residues in proximity of the spin label.

X-ray crystallography

The longer protein construct (amino acids 362–471; Figure 1) was crystallized at 293 K by the hanging drop vapor diffusion method from 1.1 µl drops of protein (11 mg/ml) and a precipitant containing 0.2 M lithium sulfate, 30% PEG 4000, 12% MPD and 0.1 M Tris (pH 8.5). The crystals were transferred to a cryoprotecting solution composed of mother liquor and 30% glycerol prior to flash freezing in liquid nitrogen. X-ray diffraction data was collected on the ID14-2 beamline at the ESRF. Data were processed using MOSFLM (CCP4, Collaborative Computational Project 4). The crystals belonged to the C2 space group with a predicted two molecules per asymmetric unit. The cell parameters and data collection statistics are reported in Table III.

The first MR attempts using either single models taken from the NMR ensemble, a minimum averaged structure or the entire NMR ensemble did not yield clear solutions. Four different models generated starting from the NMR structure and consisting of the ensemble of 50 NMR structures were used as search models in separated MR runs: (a) the 'full' model contained the full dsRBD structure and C-terminal helix but not the disordered regions of the NMR ensemble (N- and C-terminal residues plus loops 1 and 2); (b) the second model contained the same ordered residues as the 'full' model but flexible side chains (those with high r.m.s.d. in the NMR ensemble) were replaced with Ala; (c) a poly-Ala version of the 'full' model; (d) a 'truncated' model where the additional helix α3 (not present in the canonical dsRBD fold) was removed. Three MR programs were used simultaneously with each of the four search models: AMORE (Navaza, 2002), MOLREP (Vagin and Teplyakov, 1997) and BEAST (Read, 2001). The results from all three programs were compared and the solution common to all programs (not necessarily the best ranking solution in any of the programs) was chosen. The BEAST program was most efficient in separating this solution from the background noise. Search model b (full model with truncated flexible side chains) yielded the clearest solutions. The frequency of occurrence of the MR solution in three different programs and four different NMR ensembles yielded confidence.

Refinement required several cycles of non-crystallographic symmetry (NCS) phased refinement and automatic rebuilding to lower R/R_{free} to acceptable values. Eliminating the flexible regions in the ensemble and using the NCS was central to the success of both the MR and the subsequent refinement. Two molecules of the NMR ensemble closest to the mean were chosen for refinement, but initial refinement using REFMAC proved difficult. Starting values of 55% R/R_{free} did not lower significantly and inspection of electronic density maps was not helpful in determining which parts of the model were in error. This was interpreted as the manifestation of a correct phasing solution trapped in local secondary minimum. The 'NCS phased refinement' module in CCP4i was then used (CCP4, Collaborative Computational Project 4). This module iteratively performs density modification, averages the maps using the NCS and refines the model against the density-modified phases using REFMAC (Murshudov *et al*, 1999). Lower *R*-factors of 40–45% were obtained but refinement stalled again. Full model rebuilding using Arp/Warp (Perrakis *et al*, 1999) was not possible at this resolution, but multiple cycles of model rebuilding using the 'Model update and refinement' in Arp/Warp and NCS phased refinement finally allowed acceptable values of R/R_{free} to be reached. Further model building and refinement were performed using O (Jones *et al*, 1991) and REFMAC (Murshudov *et al*, 1999). NCS restraints between the two monomers in the asymmetric unit could not be used because some regions of the protein were found in different conformations. The final model of the two proteins in the asymmetric unit contains residues 361–448 and 363–443, respectively. Statistics for the data collection, MR and refinement are summarized in Table III. Atomic coordinates are deposited into the Protein Data Bank under accession numbers 1T4N (NMR) and 1T4O (X-ray).

Supplementary data

Supplementary data are available at *The EMBO Journal* Online.

Acknowledgements

Work at UC Santa Cruz was supported by the WM Keck foundation, and work at the University of Washington was supported by a grant from NIH-NIGMS. Work at Université Paris-Sud is supported by grants from the Ministère de la Recherche et de la Technologie (Programme Génopoles) and the Association pour la Recherche contre le Cancer (to M Graille).

References

Allain FH-T, Bouvet P, Dieckmann T, Feigon J (2000) Molecular basis of sequence-specific recognition of pre-ribosomal RNA by nucleolin. *EMBO J* **19:** 6870–6881

Avis J, Allain FH-T, Howe PWA, Varani G, Neuhaus D, Nagai K (1996) Solution structure of the N-terminal RNP domain of U1A protein: the role of C-terminal residues in structure stability and RNA binding. *J Mol Biol* **257:** 398–411

Bevilacqua PC, Cech TR (1996) Minor-groove recognition of the double-stranded RNA-binding domain from the RNA-activated protein kinase PKR. *Biochemistry* **35:** 9983–9994

Blaszczyk J, Gan J, Tropea JE, Court DL, Waugh DS, Ji X (2004) Noncatalytic assembly of ribonuclease III with double-stranded RNA. *Structure* **12:** 457–466

Blaszczyk J, Tropea JE, Bubunenko M, Routzahn KM, Waugh DS, Court DL, Ji X (2001) Crystallographic and modeling studies of RNase III suggest a mechanism for double-stranded RNA cleavage. *Structure* **9:** 1225–1236

Brunger AT, Adams PD, Clore GM, DeLano WL, Gros P, Grosse-Kunstelve RW, Jiang JS, Kuszewski J, Nilges M, Pannu NS, Read RJ (1998) CNS: a system for crystallography and NMR. *Acta Crystallogr D* **54:** 905–921

Bycroft M, Grünert S, Murzin AG, Proctor M, St Johnston D (1995) NMR solution structure of a dsRNA binding domain from *Drosophila* Staufen protein reveals homology to the N-terminal domain of ribosomal protein S5. *EMBO J* **14:** 3563–3571

Chanfreau G, Buckle M, Jacquier A (2000) Recognition of a conserved class of RNA tetraloops by *Saccharomyces cerevisiae* RNase III. *Proc Natl Acad Sci USA* **97:** 3142–3147

Chanfreau G, Legrain P, Jacquier A (1998) Yeast RNAse III as a key processing enzyme in small nucleolar RNAs metabolism. *J Mol Biol* **284:** 975–988

Conrad C, Rauhut R (2002) Ribonuclease III: new sense from nuisance. *Int J Biochem Cell Biol* **34:** 116–129

Danin-Kreiselman M, Lee CY, Chanfreau G (2003) RNAse III-mediated degradation of unspliced pre-mRNAs and lariat introns. *Mol Cell* **11:** 1279–1289

Dragon F, Pogacic V, Filipowicz W (2000) *In vitro* assembly of human H/ACA small nucleolar RNPs reveals unique features of U17 and telomerase RNAs. *Mol Cell Biol* **20:** 3037–3048

Elela SA, Igel H, Ares MJ (1996) RNAse III cleaves eukaryotic pre-ribosomal RNA at a U3 snoRNP-dependent site. *Cell* **85:** 115–124

Fierro-Monti I, Mathwes MB (2000) Proteins binding to duplexed RNA: one motif, multiple functions. *Trends Biochem Sci* **25:** 241–246

Filipowicz W, Pogacic V (2002) Biogenesis of small nucleolar ribonucleoproteins. *Curr Opin Cell Biol* **14:** 319–327

Gochin M (2000) A high resolution structure of a DNA–chromomycin–Co(II) complex determined from pseudocontact shifts in nuclear magnetic resonance. *Structure* **8:** 441–452

Gouet P, Courcelle E, Stuart DI, Metoz F (1999) ESPRIPT: Analysis of multiple sequence alignments in post script. *Bioinformatics* **15:** 305–308

Green SR, Matthews MB (1992) Two RNA-binding motifs in the double-stranded RNA-activated protein kinase, DAI. *Genes Dev* **6:** 2478–2490

Howe PWA, Allain FH-T, Varani G, Neuhaus D (1998) Determination of the NMR structure of the complex between U1A protein and its RNA polyadenylation inhibition element. *J Biomol NMR* **11:** 59–84

Jones TA, Zou JH, Cowan SW, Kieldgaard M (1991) Improved methods for building protein models in electron density maps and the location of errors in these models. *Acta Crystallogr A* **47:** 110–119

Kharrat A, Macias MJ, Gibson TJ, Nilges M, Pastore A (1995) Structure of the dsRNA binding domain of *E. coli* RNAse III. *EMBO J* **14:** 3572–3584

Knight SWaBBL (2001) A role for the RNase III enzyme DCR-1 in RNA interference and germ line development in *Caenorhabditis elegans*. *Science* **293:** 2269–2271

Koradi R, Billeter M, Wuthrich K (1996) MOLMOL: a program for display and analysis of macromolecular structures. *J Mol Graph* **14:** 51–55

Lamontagne B, Ghazal G, Lebars I, Yoshizawa S, Fourmy D, Elela SA (2003) Sequence dependence of substrate recognition and cleavage by yeast RNase III. *J Mol Biol* **327:** 985–1000

Lamontagne B, Tremblay A, Abou Elea S (2000) The N-terminal domain that distinguishes yeast from bacterial RNAse III contains a dimerization signal required for efficient double-stranded RNA cleavage. *Mol Cell Biol* **20:** 1104–1115

Lamontagne N, Abou Elela S (2004) Evaluation of the RNA determinants for bacterial and yeast RNAse III binding and cleavage. *J Biol Chem* **279:** 2231–2241

Lebars I, Lamontagne B, Yoshizawa S, Aboul-Elela S, Fourmy D (2001) Solution structure of conserved AGNN tetraloops: insights into Rnt1p RNA processing. *EMBO J* **20:** 7250–7258

Lee Y-F, Ahn C, Han J, Choi H, Kim J, Yim J, Lee J, Provost P, Radmark O, Ki S, Kim VN (2003) The nuclear RNAseIII Drosha initiates microRNA processing. *Nature* **425:** 415–419

Lehmann KA, Bass BL (2000) Double-stranded RNA adenosine deaminases ADAR1 and ADAR2 have overlapping specificities. *Biochemistry* **39:** 12875–12884

Lugovskoy AA, Degterev AI, Fahmy AF, Zhou P, Gross JD, Yuan J, Wagner G (2002) A novel approach for characterizing protein ligand complexes: molecular basis for specificity of small-molecule BcI-2 inhibitors. *J Am Chem Soc* **124:** 1234–1240

Murshudov GN, Vagin AA, Lebedev A, Wilson KS, Dodson EJ (1999) Efficient anisotropic refinement of macromolecular structures using FFT. *Acta Crystallogr D* **55:** 247–255

Nagel R, Ares MJ (2000) Rnt1p substrate specificity is mediated through interactions between a double-stranded RNA binding domain and a 5′-AGNN-3′ RNA loop. *RNA* **6:** 1142–1156

Nanduri S, Carpick BW, Yang Y, Williams BRG, Qin J (1998) Structure of the double stranded RNA-binding domain of the protein kinase PKR reveals the molecular basis of its dsRNA-mediated activation. *EMBO J* **17:** 5458–5465

Nanduri S, Rahman F, Williams BRG, Qin J (2000) A dynamically-tuned double-stranded RNA-binding mechanism for the activation of antiviral kinase PKR. *EMBO J* **19:** 5567–5574

Navaza J (2002) Implementation of molecular replacement in AMoRe. *Acta Crystallogr A* **58:** 568–573

Perez-Canadillas J-M, Varani G (2003) Recognition of GU-rich polyadenylation regulatory elements by human CstF-64 protein. *EMBO J* **22:** 2821–2830

Perrakis A, Morris RJ, Lamzin VS (1999) Automated protein model building combined with iterative structure refinement. *Nat Struct Biol* **6:** 458–463

Polson AG, Bass BL (1994) Preferential selection of adenosines for modification by double-stranded RNA adenosine deaminase. *EMBO J* **13:** 5701–5711

Price SR, Oubridge C, Varani G, Nagai K (1998) Preparation of RNA–protein complexes for X-ray crystallography and NMR. In *RNA–Protein Interaction: Practical Approach*, Smith C (ed) pp 37–74. Oxford: Oxford University Press

Proud CG (1995) PKR: a new name and new roles. *Trends Biochem Sci* **20:** 241–246

Ramos A, Bayer P, Varani G (2000a) Determination of the structure of the RNA complex of a double-stranded RNA-binding domain from *Drosophila* Staufen protein. *Biopolymers* **52:** 181–196

Ramos A, Grunert S, Adams J, Micklem D, Proktor M, Bycroft M, St Jhonston D, Varani G (2000b) RNA recognition by a Staufen double-stranded RNA binding domain. *EMBO J* **19:** 997–1009

Ramos A, Varani G (1998) A new method to detect long-range protein–RNA contacts: NMR detection of electron–proton relaxation induced by nitroxide spin-labeled RNA. *J Am Chem Soc* **120:** 10992–10993

Read RJ (2001) Pushing the boundaries of molecular replacement with maximum likelihood. *Acta Crystallogr D* **57:** 1373–1382

Ryter JM, Schultz SC (1998) Molecular basis of double-stranded RNA–protein interactions: structure of a dsRNA-. *EMBO J* **17:** 7505–7513

Sattler M, Schleucher J, Griesinger C (1999) Heteronuclear multidimensional NMR experiments for the structure determination of proteins in solution employing pulsed field gradients. *Prog NMR Spectrosc* **34:** 93–158

St Johnston D, Brown NH, Gall JG, Jantsch M (1992) A conserved double-stranded RNA binding domain. *Proc Natl Acad Sci USA* **89:** 10979–10983

Tremblay A, Lamontagne B, Catala M, Yam Y, Larose S, Good L, Abou Elela S (2002) A physical interaction between Gar1p and Rnt1p is required for the nuclear import of H/ACA small nucleolar RNA-associated proteins. *Mol Cell Biol* **22:** 4792–4802

Vagin A, Teplyakov A (1997) MOLREP: an automated program for molecular replacement. *J Appl Crystallogr* **30:** 1022–1025

Varani G, Nagai K (1998) RNA recognition by RNP proteins during RNA processing and maturation. *Annu Rev Biophys Biomol Struct* **27:** 407–445

Varani L, Gunderson S, Kay LE, Neuhaus D, Mattaj I, Varani G (2000) The NMR structure of the 38 kDa RNA–protein complex reveals the basis for cooperativity in inhibition of polyadenylation by human U1A protein. *Nat Struct Biol* **7:** 329–335

Wang X, Tanaka-Hall T (2001) Structural basis for recognition of AU-rich element RNA by Hu proteins. *Nat Struct Biol* **8:** 141–146

Wu H, Yang PK, Butcher SE, Kang S, Chanfreau G, Feigon J (2001) A novel family of RNA tetraloop structure forms the recognition site for *Saccharomyces cerevisiae* RNase III. *EMBO J* **20:** 7240–7249

Zamore PD (2001) Thirty-three years later, a glimpse at the ribonuclease III active site. *Mol Cell* **8:** 1158–1160